Energy conservation in the δ-SPH scheme

M. Antuono, B. Bouscasse, A. Colagrossi
Marine Technology Research Institute (CNR-INSEAN)
Rome, Italy

S. Marrone
LHEEA-ECN, Nantes, France
CNR-INSEAN, Rome, Italy

***Abstract*—An in-depth analysis of the energy conservation in the δ-SPH model has been carried on. In comparison to the standard SPH scheme, the mechanical energy equation of the δ-SPH variant is characterized by a further term that is generally dissipative and is related to the diffusive operator inside the continuity equation. The behaviour and the structure of such a term have been studied in detail and a number of specifically conceived test cases has been considered, highlighting that the dissipative term is generally small and it mainly acts when spurious high-frequency acoustic components are excited.**

I. Introduction

The δ-SPH scheme is a variant of the standard SPH model that includes a diffusive term in the continuity equation to reduce the high-frequency spurious oscillations in the pressure field. This scheme satisfies the conservation of mass and of the linear and angular momenta and, since its definitions (see [1], [2]), it has been successfully applied to several hydrodynamics problems (see [3]–[6]). In the present work we add a further contribution to the analysis of the δ-SPH scheme and study the conservation of energy in such a model.

We show that, in comparison to the standard SPH model, the mechanical energy equation of the δ-SPH scheme contains a further term that is generally dissipative and that derives from the diffusive operator inside the continuity equation. Further, we describe the general structure of such a term (hereinafter called diffusive power term) and, through numerical test cases, we draw a qualitative description of its behaviour. Specifically, we considered two test cases where the fluid is inviscid and no solid boundaries are present. Under these hypotheses, it is possible to focus on the evolution of the diffusive power term, neglecting viscous and fluid-body interactions. We observed that the magnitude of the diffusive power term is generally small and it mainly acts during the generation of shock waves or when spurious high-frequency oscillations characterize the pressure field. Since the diffusive power term principally drags energy from the compressible components of the SPH, the δ-SPH scheme appears to be somehow "less compressible" than the standard SPH.

The paper is organized as follows: section §III introduces the δ-SPH scheme and section §IV describes the main energy terms, the energy equations and define the diffusive power term. Then, sections §V and §VI show some applications of the δ-SPH to inviscid free-surface flows and describe the behaviour of the diffusive power term.

II. The standard SPH

Hereinafter we call standard SPH the following system:

$$\begin{cases} \dfrac{\mathrm{d}\rho_i}{\mathrm{d}t} = -\displaystyle\sum_j (\boldsymbol{u}_j - \boldsymbol{u}_i)\cdot\nabla_i W_{ij}\, m_j\,, \\[2ex] \dfrac{\mathrm{d}\boldsymbol{u}_i}{\mathrm{d}t} = -\displaystyle\sum_j \left(\frac{p_j}{\rho_j^2}+\frac{p_i}{\rho_i^2}\right)\nabla_i W_{ij}\, m_j + \boldsymbol{f}_i + \\[2ex] \qquad + \mu \displaystyle\sum_j \pi_{ij}\,\nabla_i W_{ij}\,\frac{m_j}{\rho_j\rho_i} \\[2ex] \dfrac{\mathrm{d}\boldsymbol{r}_i}{\mathrm{d}t} = \boldsymbol{u}_i \qquad\qquad p_i = c_0^2\,(\rho_i-\rho_0) \end{cases} \tag{1}$$

where ρ_i, p_i are respectively the density and the pressure of the $i-$particle while $\boldsymbol{r}_i$ and $\boldsymbol{u}_i$ are its position and velocity. The particle mass, m_i, is constant during the motion so that the global mass i conserved exactly. Here, W_{ij} is the kernel function (a Wendland kernel is used hereinafter), ∇_i denotes the differentiation with respect to $\boldsymbol{r}_i$ and $\boldsymbol{f}_i$ is the body force at the position $\boldsymbol{r}_i$. Finally, symbols ρ_0 and c_0 indicate the density along the free surface (which is the reference value for the density field) and the sound velocity (assumed to be constant). The dynamic viscosity is indicated through μ while the kernel of the viscous term is given in [7] and reads:

$$\pi_{ij} = K\,\frac{(\boldsymbol{u}_j-\boldsymbol{u}_i)\cdot\boldsymbol{r}_{ji}}{\|\boldsymbol{r}_{ji}\|^2}\,. \tag{2}$$

where $K = 2\,(n+2)$ and n is the number of spatial dimensions.

III. The δ-SPH scheme

The δ-SPH has been first defined in [1] and further inspected in [2]. It reads:

$$\begin{cases} \dfrac{\mathrm{d}\rho_i}{\mathrm{d}t} = -\rho_i\displaystyle\sum_j (\boldsymbol{u}_j - \boldsymbol{u}_i)\cdot\nabla_i W_{ij}\, V_j + \delta\, h\, c_0\, \mathcal{D}_i \\[2ex] \dfrac{\mathrm{d}\boldsymbol{u}_i}{\mathrm{d}t} = -\dfrac{1}{\rho_i}\displaystyle\sum_j (p_j+p_i)\,\nabla_i W_{ij}\, V_j + \boldsymbol{f}_i + \\[2ex] \qquad + \dfrac{\mu}{\rho_i}\displaystyle\sum_j \pi_{ij}\,\nabla_i W_{ij}\, V_j \\[2ex] \dfrac{\mathrm{d}\boldsymbol{r}_i}{\mathrm{d}t} = \boldsymbol{u}_i \qquad\qquad p_i = c_0^2\,(\rho_i-\rho_0) \end{cases} \tag{3}$$

Here, $V_i = m_i/\rho_i$ is the volume of the i-th particle and, similarly to the standard SPH, the mass m_i is constant during the evolution. The diffusive term is given by:

$$\mathcal{D}_i = 2 \sum_j \psi_{ji} \frac{\boldsymbol{r}_{ji} \cdot \nabla_i W_{ij}}{\|\boldsymbol{r}_{ji}\|^2} V_j \tag{4}$$

where $\boldsymbol{r}_{ji} = (\boldsymbol{r}_j - \boldsymbol{r}_i)$ and

$$\psi_{ji} = \left\{ \left(\rho_j - \rho_i\right) - \frac{1}{2} \left(\langle \nabla\rho \rangle_j^L + \langle \nabla\rho \rangle_i^L \right) \cdot \boldsymbol{r}_{ji} \right\} . \tag{5}$$

The system (3) is integrated in time by using a fourth-order Runge-Kutta scheme with frozen diffusion as described in [2]. The time step is obtain as the minimum over the following bounds:

$$\Delta t \le 0.44 \frac{h}{\delta\, c_0}, \quad \Delta t \le 0.125 \frac{h^2}{\nu}, \quad \Delta t \le 0.25 \min_i \sqrt{\frac{h}{\|\boldsymbol{a}_i\|}},$$

$$\Delta t \le CFL \min_i \left(\frac{h}{c_0 + \|\boldsymbol{u}_i\| + h \max_j |\pi_{ij}|} \right).$$

where $\|\boldsymbol{a}_i\|$ is the particle acceleration and $CFL = 2$. Generally, the last inequality is the most restrictive. To impose the weakly-compressibility assumption, the sound speed has been chosen to satisfy the following requirement:

$$c_0 \ge 10 \max\left(U_{max}, \sqrt{\frac{p_{max}}{\rho_0}} \right), \tag{6}$$

where U_{max} and p_{max} are the maximum expected velocity and pressure.

IV. The energy equations

The global kinetic energy equation is obtained by multiplying the momentum equation for $\boldsymbol{u}_i$ scalarly and by summing all over the fluid particles. Using the symmetry properties of the arguments of the summations, it is possible to rearrange the global kinetic energy equation in the following manner:

$$\frac{\mathrm{d}\mathcal{E}_K}{\mathrm{d}t} = -\frac{1}{2} \sum_i^* V_i \sum_j^* (p_j + p_i)\, (\boldsymbol{u}_i - \boldsymbol{u}_j) \cdot \nabla_i W_{ij}\, V_j +$$

$$+ \sum_i^* m_i\, \boldsymbol{u}_i \cdot \boldsymbol{f}_i + \frac{\mu K}{2} \sum_i^* V_i \sum_j^* \pi_{ij}\, (\boldsymbol{u}_i - \boldsymbol{u}_j) \cdot \nabla_i W_{ij}\, V_j + \mathcal{P}_s , \tag{7}$$

where the starred summations indicate the summations over the fluid particles and:

$$\mathcal{E}_k = \sum_i^* m_i \frac{\|\boldsymbol{u}_i\|^2}{2} . \tag{8}$$

The symbol $\mathcal{P}_s$ represents the power due to the interaction between the fluid with the solid boundaries:

$$\mathcal{P}_s = -\sum_i^* V_i \overline{\sum_j} (p_j + p_i)\, \boldsymbol{u}_i \cdot \nabla_i W_{ij}\, V_j +$$

$$+ \mu\, K \sum_i^* V_i \overline{\sum_j} \pi_{ij}\, \boldsymbol{u}_i \cdot \nabla_i W_{ij}\, V_j . \tag{9}$$

The barred summations indicate the summation over the mirror particles in the solid boundary.

If the body force is conservative, that is $\boldsymbol{f} = \nabla\phi$ with $\phi = \phi(\boldsymbol{r})$, we can extract the potential energy:

$$\sum_i^* m_i\, \boldsymbol{u}_i \cdot \boldsymbol{f}_i = \frac{\mathrm{d}}{\mathrm{d}t} \left[\sum_i^* m_i\, \phi_i \right] = -\frac{\mathrm{d}\mathcal{E}_p}{\mathrm{d}t} . \tag{10}$$

Finally, we introduce the global internal energy $\mathcal{E}_i$ with the following requirement:

$$\frac{\mathrm{d}}{\mathrm{d}t} \left(\mathcal{E}_k + \mathcal{E}_p + \mathcal{E}_i \right) = 0 . \tag{11}$$

Hereinafter, we indicate the total energy of the system by $\mathcal{E}_{tot} = \mathcal{E}_k + \mathcal{E}_p + \mathcal{E}_i$. As a consequence of (11), the equation of the internal energy reads:

$$\frac{\mathrm{d}\mathcal{E}_i}{\mathrm{d}t} = \frac{1}{2} \sum_i^* V_i \sum_j^* (p_j + p_i)\, (\boldsymbol{u}_i - \boldsymbol{u}_j) \cdot \nabla_i W_{ij}\, V_j +$$

$$- \frac{\mu K}{2} \sum_i^* V_i \sum_j^* \pi_{ij}\, (\boldsymbol{u}_i - \boldsymbol{u}_j) \cdot \nabla_i W_{ij}\, V_j - \mathcal{P}_s . \tag{12}$$

Finally, we indicate the mechanical energy of the system through $\mathcal{E}_M = \mathcal{E}_k + \mathcal{E}_p$.

A. The power of the diffusive term

Now, let us focus on the first term in the right-hand side of equation (7). Using the continuity equation and the symmetry properties, it is possible to rewrite it in the following way:

$$-\frac{1}{2} \sum_i^* V_i \sum_j^* (p_j + p_i)\, (\boldsymbol{u}_i - \boldsymbol{u}_j) \cdot \nabla_i W_{ij}\, V_j =$$

$$= \sum_i^* V_i\, p_i \sum_j^* (\boldsymbol{u}_j - \boldsymbol{u}_i) \cdot \nabla_i W_{ij}\, V_j =$$

$$= \sum_i^* V_i\, p_i \left[-\frac{1}{\rho_i} \frac{\mathrm{d}\rho_i}{\mathrm{d}t} - \overline{\sum_j} (\boldsymbol{u}_j - \boldsymbol{u}_i) \cdot \nabla_i W_{ij}\, V_j + \delta\, h\, c_0 \frac{\mathcal{D}_i}{\rho_i} \right] =$$

$$= -\sum_i^* m_i \frac{p_i}{\rho_i^2} \frac{\mathrm{d}\rho_i}{\mathrm{d}t} + \hat{\mathcal{P}}_s + \delta\, h\, c_0 \sum_i^* \frac{p_i}{\rho_i} \mathcal{D}_i V_i =$$

$$= -\frac{\mathrm{d}\mathcal{E}_C}{\mathrm{d}t} + \hat{\mathcal{P}}_s + \delta\, h\, c_0 \sum_i^* \frac{p_i}{\rho_i} \mathcal{D}_i V_i ,$$

where

$$\hat{\mathcal{P}}_s = -\sum_i^* V_i\, p_i \overline{\sum_j} (\boldsymbol{u}_j - \boldsymbol{u}_i) \cdot \nabla_i W_{ij}\, V_j , \tag{13}$$

and the symbol $\mathcal{E}_C$ indicates the reversible energy due to compressibility. In the present case, we obtain:

$$\mathcal{E}_C = \sum_i^* m_i\, c_0^2 \left[\log\left(\frac{\rho_i}{\rho_0} \right) + \frac{\rho_0}{\rho_i} \right] \tag{14}$$

Then, in comparison to the standard SPH scheme, the δ-variants predicts a further term in the global equations of

kinetic and internal energy. Specifically, the global kinetic energy equation can be rearranged in the following way:

$$\frac{\mathrm{d}}{\mathrm{d}t}\left[\mathcal{E}_K + \mathcal{E}_p + \mathcal{E}_C\right] = \mathcal{P}_\delta + \mathcal{P}_v + \mathcal{P}_s + \hat{\mathcal{P}}_s\,, \tag{15}$$

where $\mathcal{P}_\delta$ represents the power associated to the diffusive term and $\mathcal{P}_v$ is the power dissipated by viscosity:

$$\mathcal{P}_\delta = \delta\, h\, c_0 \sum_i^* \frac{p_i}{\rho_i}\,\mathcal{D}_i V_i \tag{16}$$

$$\mathcal{P}_v = \frac{\mu K}{2}\sum_i^* V_i \sum_j^* \pi_{ij}\,(\boldsymbol{u}_i - \boldsymbol{u}_j)\cdot\nabla_i W_{ij}\,V_j\,. \tag{17}$$

Differently from $\mathcal{P}_v$ (which is always negative for the second principle of thermodynamics), $\mathcal{P}_\delta$, $\mathcal{P}_s$ and $\hat{\mathcal{P}}_s$ have not a defined sign. In the sequel, we show through numerical simulations that $\mathcal{P}_\delta$ is negative as well and, therefore, it represents a dissipation.

Before proceeding to the analysis, it is convenient to introduce some further concepts. As a consequence of equation (11), we can write:

$$\frac{\mathrm{d}}{\mathrm{d}t}\left[\mathcal{E}_i - \mathcal{E}_C\right] = -\mathcal{P}_\delta - \mathcal{P}_v - \mathcal{P}_s - \hat{\mathcal{P}}_s\,. \tag{18}$$

Hereinafter, we indicate the irreversible energy of the system by $\mathcal{E}_{irr} = \mathcal{E}_i - \mathcal{E}_C$ and the reversible energy of the system by $\mathcal{E}_{rev} = \mathcal{E}_k + \mathcal{E}_p + \mathcal{E}_C$. Integrating in time equations (15) and (18), we obtain:

$$\mathcal{E}_{rev}(t) - \mathcal{E}_{rev}(t_0) = -\mathcal{Q}_\delta - \mathcal{Q}_v - \mathcal{Q}_s - \hat{\mathcal{Q}}_s\,,$$

$$\mathcal{E}_{irr}(t) - \mathcal{E}_{irr}(t_0) = \mathcal{Q}_\delta + \mathcal{Q}_v + \mathcal{Q}_s + \hat{\mathcal{Q}}_s\,,$$

where the following convention is used to indicate the heat $\mathcal{Q}$:

$$\mathcal{Q}_\delta = -\int_{t_0}^{t}\mathcal{P}_\delta\,d\tau\,,\quad \mathcal{Q}_v = -\int_{t_0}^{t}\mathcal{P}_v\,d\tau\,,$$

$$\mathcal{Q}_s = -\int_{t_0}^{t}\mathcal{P}_s\,d\tau\,,\quad \hat{\mathcal{Q}}_s = -\int_{t_0}^{t}\hat{\mathcal{P}}_s\,d\tau\,.$$

Then, a positive sign for the heat means that the fluid system is loosing reversible energy and is increasing the irreversible energy. Since the main subject of the present analysis is the δ-SPH scheme, we avoid simulations with solid boundaries, so that we can always put $\mathcal{P}_s = \hat{\mathcal{P}}_s = 0$.

V. Oscillating drop under a central conservative force field

In the present section we consider a two-dimensional fluid drop evolving under the action of a central conservative force field, $-B^2\,\boldsymbol{r}$, where B is a dimensional parameter. The fluid is inviscid (i.e. $\mu = 0$, $\mathcal{P}_v = 0$) and the drop is initially circular with radius R. The drop evolves periodically as an oscillating fluid ellipse, according to the following law:

$$\begin{cases} u = A(t)\,x \\ v = -A(t)\,y\,, \end{cases} \tag{19}$$

where the solution for $A(t)$ is given in [8]. It is simple to show that the global dynamics depends on the ratio $A(0)/B$, which, in the following simulations, is set equal to 1. According to (6), the sound velocity has been set equal to $15\,A(0)\,R$.

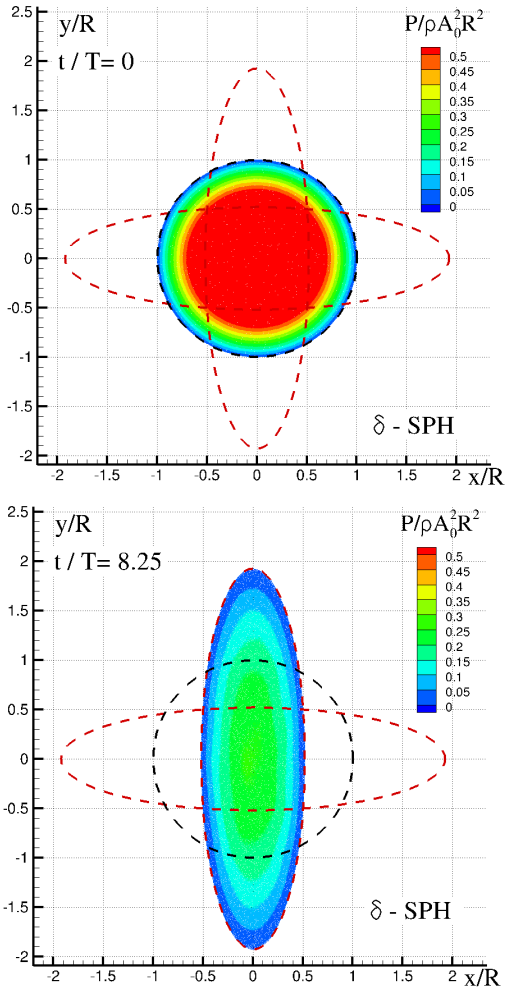

Fig. 1. Oscillating drop. Initial (right plot) and final instant (left plot) of the evolution. The dashed lines indicate the analytic solution of the free surface ($R/\Delta x = 100$).

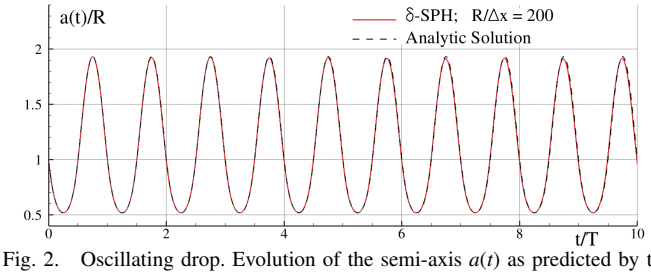

Fig. 2. Oscillating drop. Evolution of the semi-axis $a(t)$ as predicted by the δ-SPH ($R/\Delta x = 200$). The dashed line represents the analytic solution.

Figure 1 displays the initial and the final instant of the evolution obtained by using the δ-SPH scheme and the analytic solution of the free surface (dashed lines). The overall comparison is very good and it is further confirmed in figure 2, where the δ-SPH solution is compared with the analytic solution for the ellipse semi-axis, $a(t)$. At a first glance, the simulation seems to preserve energy but is not. Figure 3

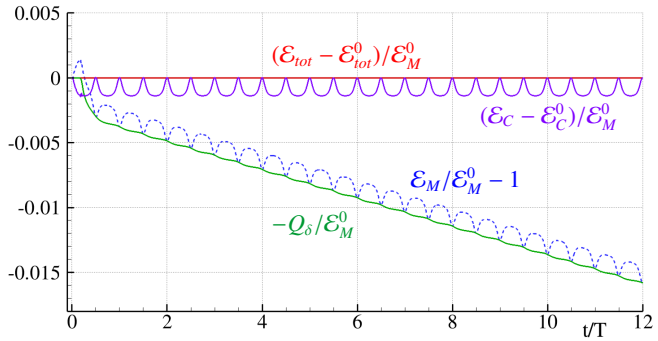

Fig. 3. Oscillating drop. Energy components of the δ-SPH scheme ($R/\Delta x = 200$). The superscript '0' indicates the initial value of the corresponding energy component.

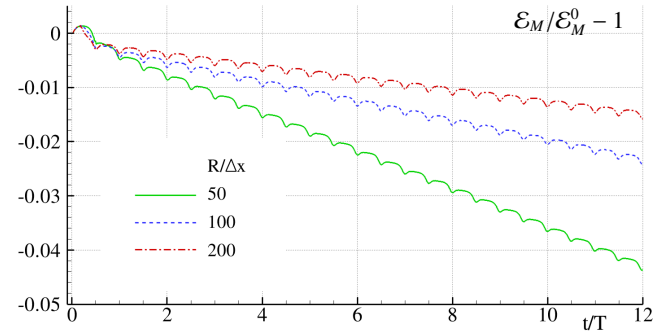

Fig. 5. Oscillating drop. Evolution of $\mathcal{E}_M$ for different spatial resolutions (δ-SPH). The superscript '0' indicates the initial value of the corresponding energy component.

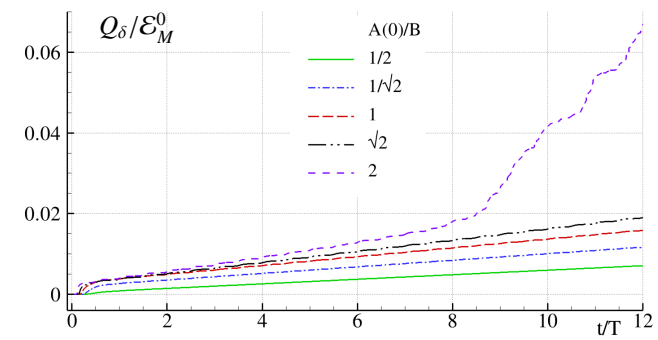

Fig. 4. Oscillating drop. Evolution of $\mathcal{Q}_\delta$ for different values of $A(0)/B$ (δ-SPH with $R/\Delta x = 200$). The symbol $\mathcal{E}_{M0}$ indicates the initial value of the mechanical energy.

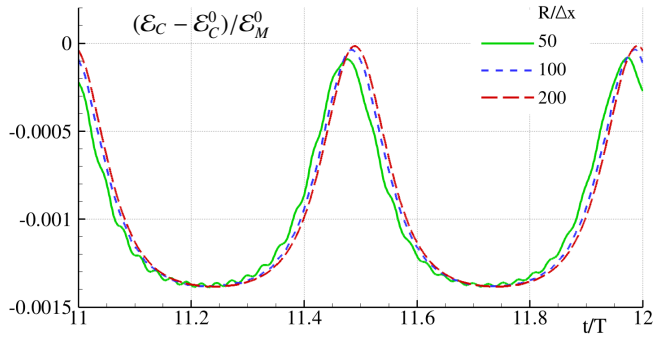

Fig. 6. Oscillating drop. Evolution of $\mathcal{E}_C$ for different spatial resolutions (δ-SPH). The superscript '0' indicates the initial value of the corresponding energy component.

shows that $\mathcal{Q}_\delta$ is always positive and, therefore, represents a dissipation. In any case, it is generally small and, in the time range here considered, it corresponds to few percentages of the initial mechanical energy.

Figure 3 also displays the time histories of the compressible and total energy. The latter one is obtained by integrating each term in equation (11) numerically. This procedure allows us to check if the time-integrator is affected by spurious dissipations and to control the accuracy of the simulation. In the present case, the time history of the total energy is practically constant and no spurious dissipation occurs. The compressible energy $\mathcal{E}_C$ is periodic and maintains always small, this confirming that the weakly-compressibility assumption is satisfied.

Figure 4 displays the evolution of $\mathcal{Q}_\delta$ for increasing values of the ratio $A(0)/B$, that is for increasing elongations. As expectable, the energy dissipated by the diffusive term increases as the deformation/elongation of the drop increases. An opposite behaviour is observed as the spatial resolution becomes finer and finer (see figure 5). This further confirms the consistency of the δ-SPH with the compressible Euler Equations for h going to zero. In all the cases shown above, the compressible energy maintains small and tends to a converged solution (see figure 6).

The analysis of the energy components is repeated by using the standard SPH ($\delta = 0$ and, consequently, $\mathcal{P}_\delta = 0$) with $A(0)/B = 1$. In this case, the simulations are more noisy and this leads to the occurrence of spurious dissipation in the time integration (see figure 7). Despite this phenomenon decreases as the spatial resolution increases (figure 8), the *CFL* number has been reduced to 0.1 to make the integration errors negligible. The conservation of the total energy is displayed in figure 9 and confirms the accuracy of the time-integration. Apart from this, figure 9 also shows an interesting behaviour of the standard SPH: a defined increase of the compressible energy at the expense of the mechanical energy. Such a phenomenon tends to disappear for increasing spatial resolutions (see figure 10) but it is always present and seems to suggest an "irreversible" energy flux from the mechanical to the compressible energy. This is quite surprising since the equations of the standard SPH are reversible (no viscosity, nor diffusion are introduced in the numerical scheme). To be sure that such a behaviour is not caused by the Runge-Kutta time integrator, we repeat the simulations by using the symplectic integrator described in [9] but obtained the same results. A possible explanation to this phenomenon may be probably given only in terms of statistical mechanics (see, for example, [10], [11]). In any case, this, at the moment, goes far beyond the aim of the present work.

VI. The impact of two rectangular fluid patches

In the present section we consider the impact of two rectangular fluid patches. Similarly to the previous section, the fluid is assumed to be inviscid and barotropic.

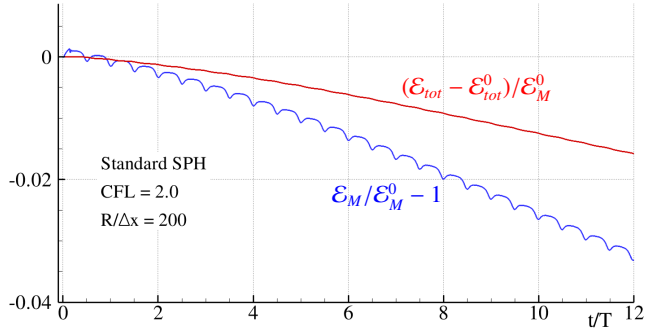

Fig. 7. Oscillating drop. Evolution of $\mathcal{E}_M$ for $A(0)/B = 1$ with the standard SPH ($R/\Delta x = 200$). The superscript '0' indicates the initial value of the corresponding energy component.

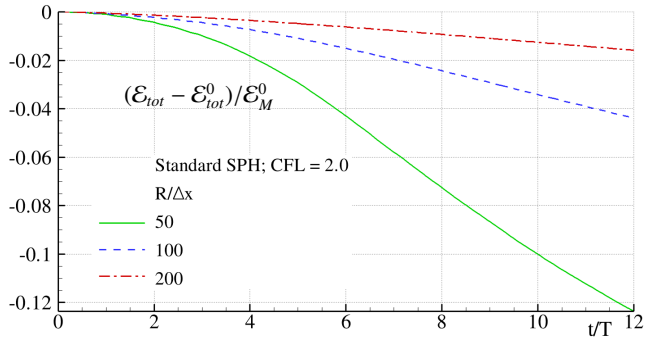

Fig. 8. Oscillating drop. Evolution of $\mathcal{E}_{tot}$ for $A(0)/B = 1$ with the standard SPH and different spatial resolutions. The superscript '0' indicates the initial value of the corresponding energy component.

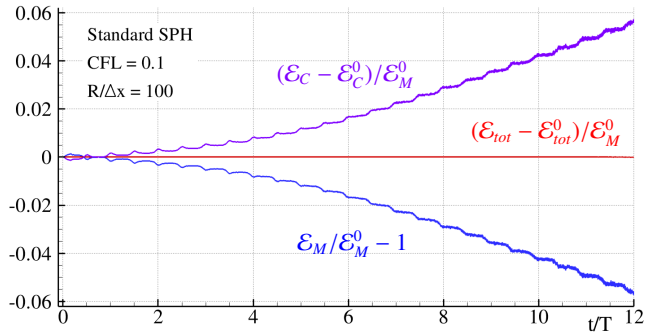

Fig. 9. Oscillating drop. Evolution of $\mathcal{E}_M$ for $A(0)/B = 1$ with the standard SPH ($R/\Delta x = 100$) and $CFL = 0.1$. The superscript '0' indicates the initial value of the corresponding energy component.

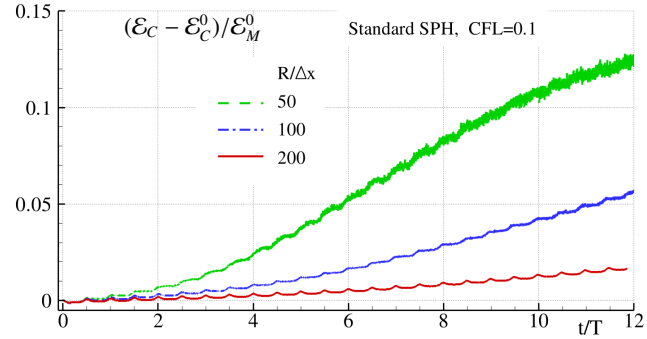

Fig. 10. Oscillating drop. Evolution of $\mathcal{E}_C$ for $A(0)/B = 1$ with the standard SPH and different spatial resolutions ($CFL = 0.1$). The superscript '0' indicates the initial value of the corresponding energy component.

Figure 11 displays some snapshots of the evolution and compares the solutions obtained by using the δ-SPH (upper half of the fluid domain) and the standard SPH (lower half of the fluid domain). The initial stages are very similar: two shock waves generate just after the impact (right upper panel of figure 11) and are followed by two rarefaction waves (left lower panel of figure 11). During the evolution, these waves are reflected at the free surface and combine together in a very complex manner. Because of the weakly-compressibility assumption, high-frequency oscillations are generated in the pressure field and propagate in the fluid bulk. These are smoothed out by the δ-SPH while, on the contrary, they persist in the standard SPH (right lower panel of figure 11).

In figure 12 we show the evolution of the mechanical energy for the δ-SPH at different spatial resolutions and the analytic solution for an incompressible fluid (see [12]). Note that the latter one is characterized by a sudden drop of the mechanical energy due to the incompressibility condition (see, for example [13]). The global evolution is made by a transitory in which the diffusive term smooths out the high-frequency oscillations of the pressure field. During this stage, the diffusion leads to an increase of Q_δ (see figure 13) and to a corresponding decrease of the compressible energy (see figure 14). Remarkably, after the transitory stage (whose duration decreases as the spatial resolution increases), the δ-SPH approaches the analytic solution. This is a remarkable point, since it means that the diffusive term is not dissipating any more (see figure 13) and confirms that it mainly acts against the high-frequency oscillations caused by the weakly-compressibility assumption.

The above analysis has been repeated by using the standard SPH. Figure 15 shows that the mechanical energy decreases after the initial impact but does not converge toward the analytic solution. Such a decrease corresponds to an equivalent increase of the compressible energy $\mathcal{E}_C$ that, similarly to the stretching drop described in the previous section, is accumulated during the evolution and it is not transformed back in mechanical energy. Again, the use of the diffusive term seems to prevent such a behaviour.

As a final example, we consider the standard SPH with the artificial viscosity proposed in [7]. Hereinafter such a scheme is denoted by α-SPH and the viscous parameter α is set equal to 0.01. Figure 16 displays the evolution of the mechanical energy for different spatial resolutions. In this case, the phenomenon of accumulation of $\mathcal{E}_C$ disappears but the use of the artificial viscosity leads to an excessive loss of mechanical energy. Apart from this, the α-SPH tends to the analytic solution as the spatial resolution becomes finer and finer (i.e., as α tends to zero). It seems that the use of a small viscosity (similarly to the use of the diffusive term) may prevent the accumulation of the compressible energy shown by the inviscid standard SPH.

VII. Conclusion

The energy components of δ-SPH scheme have been analysed in detail, highlighting the presence of a diffusive

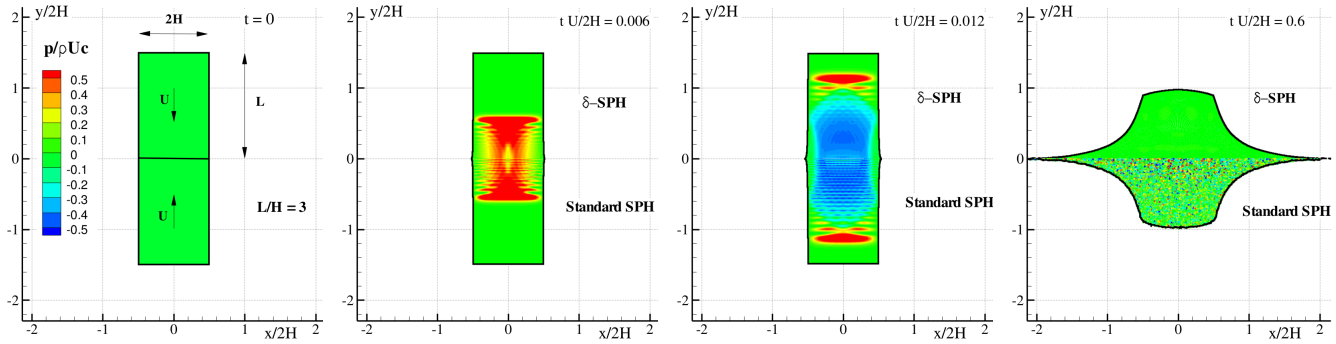

Fig. 11. The impact of two rectangular fluid patches: sketches of the evolution. The upper part of the fluid domain is given by the δ-SPH while the lower part is obtained by using the standard SPH

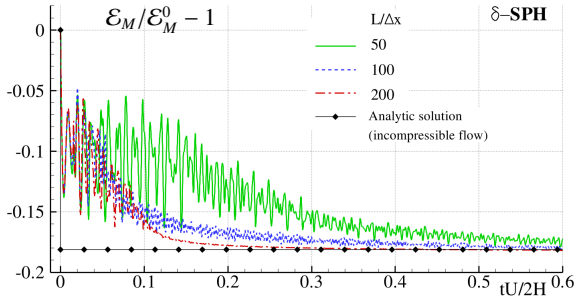

Fig. 12. The impact of two rectangular fluid patches: evolution of the mechanical energy as predicted by the δ-SPH for different spatial resolutions.

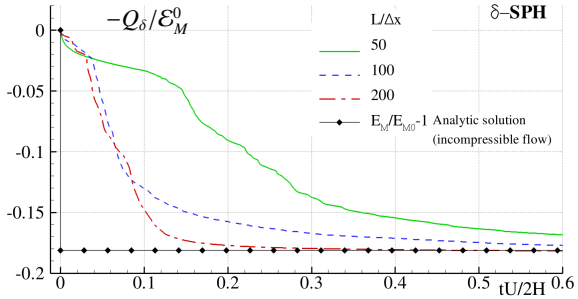

Fig. 13. The impact of two rectangular fluid patches: evolution of Q_δ as predicted by the δ-SPH for different spatial resolutions.

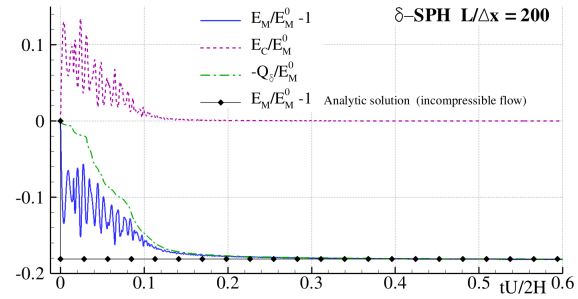

Fig. 14. The impact of two rectangular fluid patches: energy components as predicted by the δ-SPH for $L/\Delta x = 200$.

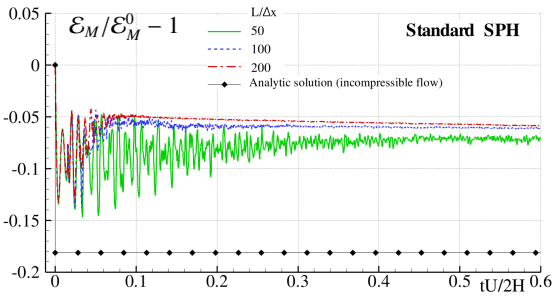

Fig. 15. The impact of two rectangular fluid patches: evolution of the mechanical energy as predicted by the standard SPH for different spatial resolutions.

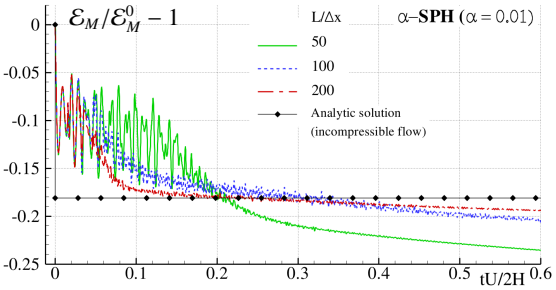

Fig. 16. The impact of two rectangular fluid patches: evolution of the mechanical energy as predicted by the α-SPH for different spatial resolutions.

power term in the mechanical energy equation that generally behaves as a dissipative contribution. Such a term mainly works against the compressibility features of the SPH, reducing the high-frequency spurious oscillations in the pressure field and preventing an eventual accumulation of mechanical energy as compressible energy $\mathcal{E}_C$. Its action generally leads to an increase of the internal energy of the system which is, however, limited to the stages of the evolution when the compressibility of the fluid is more excited. For this reason, the δ-SPH is just slightly more dissipative than the standard SPH while, in turn, it appears to be less compressible and more accurate.

Acknowledgment

The research leading to these results has received funding by the Flagship Project RITMARE - The Italian Research for the

Sea - coordinated by the Italian National Research Council and funded by the Italian Ministry of Education, University and Research within the National Research Program 2012-2014. The work was supported also by Region Pays de la Loire under the grant n. 2012-12072.

References

[1] M. Antuono, A. Colagrossi, S. Marrone, D. Molteni, *Free-surface flows solved by means of SPH schemes with numerical diffusive terms*, Computer Physics Communications, **181**, 532-549, (2010).

[2] M. Antuono, A. Colagrossi, S. Marrone, *Numerical diffusive terms in weakly-compressible SPH schemes*, Computer Physics Communications, **183**: 2570-2580 (2012)

[3] S. Marrone, M. Antuono, A. Colagrossi, G. Colicchio D. Le Touzé, G. Graziani, *δ-SPH model for simulating violent impact flows*, Comput. Methods Appl. Mech. Engrg., **200**: 1526-1542 (2011)

[4] M. Antuono, A. Colagrossi, S. Marrone, C. Lugni, *Propagation of gravity waves through an SPH scheme with numerical diffusive terms*, Computer Physics Communications, **182**: 866-877 (2011)

[5] B. Bouscasse, M. Antuono, A. Colagrossi, C. Lugni *Numerical and Experimental Investigation of Nonlinear Shallow Water Sloshing*, Int. J. Nonlinear Sci. Numer. Simul., **14**(2): 123-138 (2013)

[6] S. Marrone, A. Colagrossi, M. Antuono, G. Colicchio, G. Graziani, *An accurate SPH modeling of viscous flows around bodies at low and moderate Reynolds numbers*, Journal of Computational Physics, **245**: 456-475 (2013)

[7] J.J. Monaghan, R.A. Gingold, *Shock simulation by the particle method SPH*, J. Comput. Phys., **52**, 374-389 (1983)

[8] J. J. Monaghan and Ashkan Rafiee, *A simple SPH algorithm for multi-fluid flow with high density ratios*, Int. J. Numer. Meth. Fluids, **71**: 537-561 (2013)

[9] J.J. Monaghan, *Smoothed Particle Hydrodynamics*, Rep. Prog. Phys. **68**, 1703–1759, (2005).

[10] W.G. Hoover, T.G. Pierce, C.G. Hoover, J.O. Shugart, C.M. Stein, A.L. Edwards, *Molecular Dynamics, Smoothed-Particle Applied Mechanics, and Irreversibility*, Computers Math. Applic., **28**(10-12): 155-174 (1994)

[11] H.A. Posch, W.G. Hoover, O. Kum, *Steady-state shear flows via nonequilibrium molecular dynamics and smoother-particle applied mechanics*, Physical Review Letter E, **52**(2), 1711-1729 (1995)

[12] S. Marrone, D. Le Touzé, A. Colagrossi, A. Di Mascio, *On the model inconsistencies in simulating breaking wave with mesh-based and particle methods*, 9-th international SPHERIC workshop, Paris, France, June, 03-05 2014

[13] W. Szymczak, *Energy losses in non-classical free surface flows* in Bubble Dynamics and Interface Phenomena, ser. Fluid Mechanics and Its Applications, J. Blake, J. Boulton-Stone, and N. Thomas, Eds. Springer Netherlands, 1994, vol. 23, pp. 413-420.